Fall 2015

1-D coordination polymer of transition metal as a precursor to generate surface active transition metal catalyst

Siddharth Gopalakrishnan

Department:

1-D COORDINATION POLYMER OF TRANSITION METAL AS A PRECURSOR TO GENERATE SURFACE ACTIVE TRANSITION METAL CATALYST

by

SIDDHARTH GOPALAKRISHNAN

A THESIS

Presented to the Faculty of the Graduate School of the

MISSOURI UNIVERSITY OF SCIENCE AND TECHNOLOGY

In Partial Fulfillment of the Requirements for the Degree

MASTER OF SCIENCE IN CHEMICAL ENGINEERING

2015

Approved by

Dr. Xinhua Liang, Advisor

Dr. Amitava Choudhury, Co-Advisor

Dr. Parthasakha Neogi

ABSTRACT

The work describes the synthesis, characterization and properties of Ni, Co and Cu based 1-D coordination polymer with 1, 4-benzenedicarboxylic acid as linker and 1-methylimidazole as co-ligand. The structure of the coordination polymers were investigated employing SCXRD and showed the formation of supramolecular 3-D architecture of the 1-D coordination polymer through non covalent CH..π, π.. π, and H-bonding interaction. These 1-D coordination polymers were further characterized by IR spectroscopy and thermogravimetric analysis. Thermal decomposition of these polymeric metal complexes gave rise to carbon coated metal and metal carbides nanoparticles, for the 1-D structures of Co and Ni respectively. These 1-D coordination polymer-derived metal/metal carbide-carbon composites were further characterized by Raman spectroscopy, XPS, SEM, TEM and surface area measurement. A model organic reduction reaction, the conversion of para-nitro phenol to para-amino phenol was used to demonstrate the catalytic activity of nanoparticles. The results indicated that the carbon embedded cobalt nanoparticles were excellent catalyst for reduction reaction and evolved as a promising candidate for gas phase reduction process.

ACKNOWLEDGMENTS

First and foremost, I express my sincerest gratitude to my advisors, Dr. Amitava Choudhury and Dr. Xinhua Liang, for the completion of my thesis work. I am very grateful to Dr. Amitava Choudhry for allowing me to join his research group and start working on a thesis topic. It is due to his intellectual insight and his continuous support that the thesis was completed in a timely manner. I thank Dr. Xinhua Liang for his constant support and encouragement over the period of two years. I also thank Dr. Parthasakha Neogi for being in my committee along with my advisors. I am thankful to the faculty and staff of the Chemical Engineering and Chemistry Department of Missouri University of Science and Technology for helping me grow as a student over the period of two years. I would also like to thank the staff of the Materials Research Centre for their instrument access on a regular basis. I am indebted to my fellow lab mates Dr. Anand Pariyar and Hooman Yaghoobnejad Asl, for their constant help and support. I am also thankful to Rajankumar Patel for his help with surface area measurement.

Lastly, I would like to express my gratitude to my parents, Gopalakrishnan Jambulingam and Deepa Gopalakrishnan, and my sister, Parkavee Gopalakrishnan, and all my friends for their consistent motivation and support over the last two years.

TABLE OF CONTENTS

LIST OF ILLUSTRATIONS

Figure

LIST OF TABLES

NOMENCLATURE

Symbol	Description
DMF	N, N′- dimethyformamide
Mim	N-methyl imidazole
EtOH	Ethanol
H_2BDC	1,4-benzene dicarboxylic acid
SCXRD	Single-crystal X-ray diffraction
PXRD	Powder X-ray diffraction
TGA	Thermo-gravimetric analysis
FT-IR	Fourier transformed Infra-red spectroscopy
UV-Vis	Ultraviolet-visible spectroscopy
SEM	Scanning electron microscopy
XPS	X-ray Photoelectron Spectroscopy
TEM	Transmission Electron Microscope
MOF’s	Metal Organic Frameworks
CP’s	Coordination polymers
SCC	Supramolecular coordination complex

1. INTRODUCTION

The use of metal organic frameworks (MOF's) as a favorable precursor or template in the development of new functional materials is on the rise, [1-2]. MOF's and porous hybrid solids have structured nanoporous carbon, metal nanoparticles, and metal/oxide or metal/carbon composites on decomposition, [2]. These MOF's-derived functional materials are known to give exceptionally better attributes, mostly because of inherent porosity and high surface area, originated through crystalline periodic MOF's, [1,3]. This precursor route is usually inexpensive and offers high tunability in synthetic processes, but is known to form impure phases with heterogeneous distribution of products, [1-4]. A shift of precursor from 3-D MOF's to 1-D coordination polymers (CP's) is expected to reduce the decomposition temperature considerably and may reduce the size of product distribution and can improve selectivity. However, the challenge in rational design and construction of novel coordination polymer is in itself an exciting field in the area of supramolecular chemistry and crystal engineering, [5]. The knowledge of possible topologies, the functionality of multi-topic organic linker molecules, as well as the understanding of typical metal coordination environments or the formation conditions of typical inorganic building blocks help one to understand and direct the synthesis efforts, [6]. However, the main challenge in supramolecular coordination complex (SCC) synthesis is to establish right synthetic conditions that eventually will lead to formation of defined inorganic building blocks with desired organic linker, [7]. Recent use of transition metal polycarboxylates as a precursor for post synthesis of modified high performing catalysts for practical application makes it an obvious choice for the study, [8]. Multicarboxylate

ligands have been widely used for exhibiting various coordination modes to generate structures with various building blocks such as honeycomb, brick wall, rectangular grid, bilayer, ladder, diamonds network as well as open frameworks, [9]. As bridging ligands, polycarboxylates are widely used in the assembly of supramolecular architectures because of their diverse coordination modes and bridging ability, [9, 10]. 1,4-benzenedicarboxylic acid (BDC), an aromatic polycarboxylate, which is used extensively as bridging ligands in the production of inorganic-organic hybrid materials and has been studied for its potential applications in gas storage, catalysis, separations and molecular recognition, [11].

With the underlying principle, this paper herein reports the design of three 1-D polymeric transition metal complexes as precursors for transition metal/metal carbide nanostructures coated with carbon. The thesis contains the details of methods by which the 1-D co-ordination complexes are prepared using metal salts, a polydentate ligand and a co-ligand in solution investigation of their structures employing single crystal X-ray crystallography, nature and composition of their decomposition products and their use in catalysis.

2. EXPERIMENTAL SECTION

2.1. MATERIALS AND PHYSICAL MEASUREMENTS

Cobalt nitrate ($Co(NO_3)_2 \cdot 6H_2O$), nickel chloride ($NiCl_2 \cdot 6H_2O$), copper chloride ($CuCl_2 \cdot 2H_2O$), para-nitrophenol and sodium borohydride were purchased from Alfa Aesar. 1,4-benzene dicarboxylic acid and 1- methyl imidazole were purchased from Sigma Aldrich. All chemicals and solvents were used without purification unless otherwise mentioned. Para-nitrophenol was recrystallized twice from hot water before use.

Single-crystal X-ray diffraction intensity data sets were collected on a Bruker Smart Apex diffractometer with monochromated Mo Kα radiation (0.7107 Å). Suitable crystal were selected and mounted on a glass fiber using epoxy-based glue. The data were collected at 220K employing a scan of 0.3° in ω with an exposure time of 20 s per frame. The data sets were collected using SMART software [12], the cell refinement and data reduction were carried out with SAINT [13], while the program SADABS [13] was used for the absorption correction. The structure was solved by direct methods using SHELX-97 and difference Fourier syntheses, [14]. Full-matrix least-squares refinement against |F 2| was carried out using the SHELXL-2014 using WINGX programs suite, [14].

Powder X-ray diffraction (PXRD) patterns were obtained from a PANalytical X'Pert Pro diffractometer equipped with a Cu $K\alpha_{1,2}$ anode and a linear array PIXcel detector over a 2θ range of 5° to 90° with an average scanning rate of $0.0472^{o}\ s^{-1}$.

Thermo-gravimetric analysis (TGA) was performed on the samples with a TA instrument's Q50 TGA with a scan rate of 10 °C/ min under N_2 flow rate of 40 mL/min.

FT-IR spectrum was collected using Thermo Nicolet Nexus 470 FT-IR spectrometer over 400–4000 cm^{-1} on samples embedded in KBr pellet.

UV-Vis spectroscopy was performed in Varian-Cary spectrophotometer with a scan rate of 400 nm/min.

Scanning electron microscopy (SEM) imaging was taken using Helios Nanolab-600 equipped with Energy Dispersive Spectrometry (EDS) detector (Oxford Instrument) for elemental analysis.

X-ray Photoelectron Spectrometry (XPS) was performed on a Kratos Axis 165 Photoelectron Spectrometer. The binding energies of all peaks were corrected as compared with reference peak of adventitious carbon (C1s, 284.8 eV), [15].

TEM images were obtained on FEI Tecnai F20 and Tecnai Osiris TEM operating at 200 kV. The “as prepared” sample was dispersed in an acetone solution to prepare the TEM sample. A drop of the “as prepared” solution was placed onto a carbon coated TEM grid and dried in air prior to TEM imaging and EDS. High resolution TEM was obtained with the Tecnai Osiris operated at 200 keV with a probe current of 2.5 nA. The Fast Fourier Transform (FFT) patterns generated from the lattice fringes demonstrated the crystalline character of the individual regions.

Raman Spectroscopy was performed in Lab RAM Aramis Horiba Jobin Yvom spectrometer using HeNe laser with 30sec exposure time.

Pyrolysis of the samples was carried out by chemical vapor deposition oven, and nitrogen gas and forming gas (95%N_2 and 5%H_2) were used to conduct pyrolysis.

2.2. SYNTHESIS

2.2.1. Synthesis of [Co(BDC)(Mim)$_2$]n [1]. $Co(NO_3)_2 \cdot 6H_2O$ (0.2910 g, 1 mmol), 1,4-benzenedicarboxylic acid (0.1661 g, mmol) and N-methylimidazole (0.18 ml, 2.26 mmol) were stirred with 8 mL of a DMF and EtOH solution (3:1 by volume) at room temperature. After all the solutes were dissolved, the solution was sealed in a 15 mL glass vial and placed in a preheated oven at 100°C for 24 hours, giving dark purple crystals. The crystals were washed repeatedly with DMF followed by EtOH, to remove unreacted ligands/metal salts and dried in air. Yield=42%. Fig. 2.1 shows the Cobalt Coordination complex. CHN elemental analysis for $C_{16}H_{16}N_4O_4Co$: Calculated (%)- C 49.62; H 4.16; N 14.47: Found C 49.75; H 4.32; N 14.34. FT-IR (KBr, cm^{-1}): 652, 739, 834, 1094, 1360, 1425, 1588, 2963 and 3125.

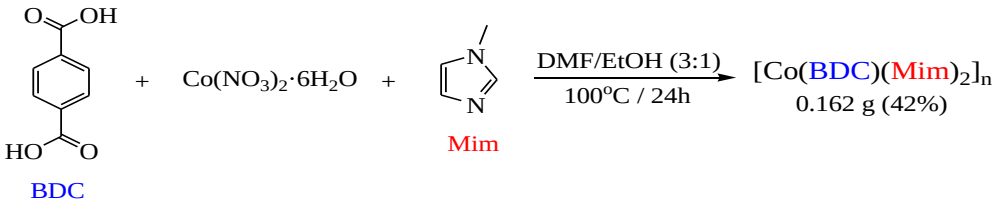

Fig. 2.1. Synthesis of Cobalt Coordination Complex

2.2.2. Synthesis of [Ni(BDC)(Mim)$_2$]n [2]. $NiCl_2 \cdot 6H_2O$ (0.2377 g, 1 mmol), 1,4-benzenedicarboxylic acid (0.1661 g, 1 mmol) and N-methylimidazole (0.16 ml, 2 mmol) were stirred into 8 mL of a DMF and EtOH solution (3:1 by volume) at room temperature. After all the solutes dissolved, it was then sealed in a HDPE bottle and placed in a preheated oven at 100°C for 24 hours, giving green crystals. The crystals were washed repeatedly with DMF followed by EtOH, to remove unreacted ligands and dried in air. Yield=34%.

Fig. 2.2 shows the Nickel Coordination complex. CHN elemental analysis for $C_{16}H_{16}N_4O_4Ni$: Calculated (%)- C 49.65; H 4.17; N 14.48: Found C49.86; H 4.35; N 14.25. FT-IR (KBr, cm^{-1}): 654, 748, 825, 1108, 1362, 1428, 1603, 2950 and 3137.

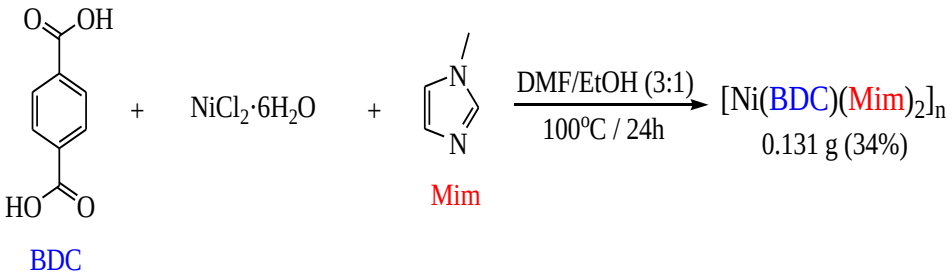

Fig. 2.2. Synthesis of Nickel Coordination Complex

2.2.3. Synthesis of [Cu(BDC)(Mim)$_2$]n [3]. $CuCl_2 \cdot 2H_2O$ (0.1705 g, 1 mmol) dissolved in 2 mL EtOH and was added to 1,4-benzene dicarboxylic acid (0.1661 g, 1 mmol) in 6 mL of DMF and the mixture was stirred in a magnetic stirrer for 10 min. The resulting mixture was blue in color which turned purple on addition of 1-methylimidazole (0.16 mL, 2 mmol). The purple mixture was stirred for another 10 min and was kept in a preheated oven heated at 100°C for 24 hours, giving purple crystals. The crystals were washed repeatedly with DMF followed by EtOH, to remove unreacted ligands and dried in air. Yield=44%. Fig. 2.3 shows the Copper Coordination complex. CHN elemental analysis for $C_{16}H_{16}N_4O_4Cu$: Calculated (%)- C 49.04; N 4.12; H 14.30: Found C49.26; H 4.29; N 14.21. FT-IR (KBr, cm^{-1}): 658, 746, 841, 1010, 1110, 1355, 1400, 1560, 1650, 2960 and 3130.

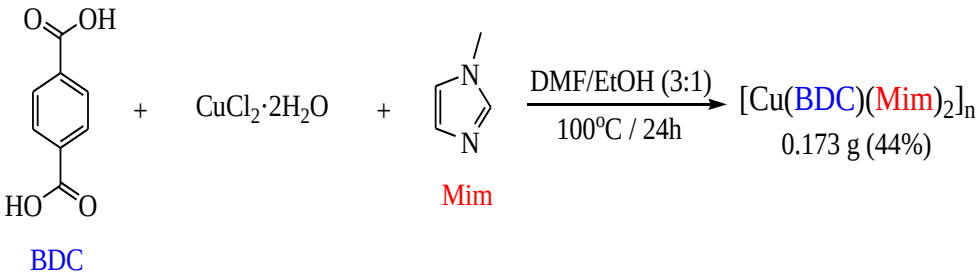

Fig. 2.3. Synthesis of Copper Coordination Complex

3. RESULTS AND DISCUSSION

3.1. SYNTHESIS AND CHARACTERIZATION OF 1-D CP'S

3.1.1. Single-Crystal X-ray Diffraction. The polymeric complexes were obtained as a pure phase by reaction of equivalent amount of metal salt and BDC (H_2BDC = benzene dicarboxylic acid) in DMF/ EtOH solvent mixture and in the presence of 2 equiv. of Mim (Mim=N-methylimidazole) as co-ligand at 100^o C for 24 hours (*See experimental section for synthetic details*). The reaction itself produced crystalline solid suitable for single crystal X-ray diffraction, and was found to be stable in air, water and organic solvents. In case of cobalt, the product crystallizes in triclinic, P-ī space group and shows the formation of polymeric coordination complex with $[Co(BDC)(Mim)_2]_n$ (1) formula unit (Table 1). The BDC ligand in 1 is coordinated to tetrahedral Co in *bis*-monodentate (*syn-anti*) fashion along with two Mim unit (Fig. 3.1). The polymeric 1-D chain is propagated *via* bridging BDC connecting Co atom in a zig-zag fashion (Fig. 3.1b). The Co(1)-Co(1')-Co(1'') angle is 100.56(1)° and the distance between two Co centers is 10.74(8) Å and 10.94(7) Å depending on the oxygen it is bonded to, O1 for the former and O3 for the latter (Table 1.1-1.4, Appendix). This is related to the fact that the Co-O1 and the Co-O3 bond lengths are 2.007(2) Å and 2.0083(18) $Å_2$ respectively which is typical for a tetrahedral Co(II) ion bonded to carboxylate ion, [16]. The Co(II) oxidation state is further supported by Co-N bond length of 2.029(2)Å (Co1-N1) and 2.056(2)Å(Co1-N3), [16]. Similar chain like structures are reported in other Cu, Zn and Ni complexes with bridged BDC where the M-M-M (M = metal) angles ranges between 65^o to ideal 120^o and are noted to be a function of steric contribution from the co-ligand, [17]. The 1-D polymeric complex 1 packs as

infinite chains along ‘a’ axis *via* inter-chain hydrogen bonding to form 2-D array (Fig. 3.1c). Two strong hydrogen bonding of distance 2.59Å (C10-H10A…O2) and 2.55Å (C12-H12C…O1) with D-H…A (D-H…A = Donor-Hydrogen…Acceptor) angle of 167^{o} and 160$^{o}{}_{2}$ respectively, were noted between the N-methyl hydrogens from Mim (Table 1.3, Appendix) group and the metal coordinated carboxylate oxygen. Furthermore, the 2-D layers give rise to 3-D supramolecular network (Fig. 3.1d) *via* CH…π interactions (Table 1.4, Appendix) evident from C-H..π distance of 2.83Å to 2.93Å.

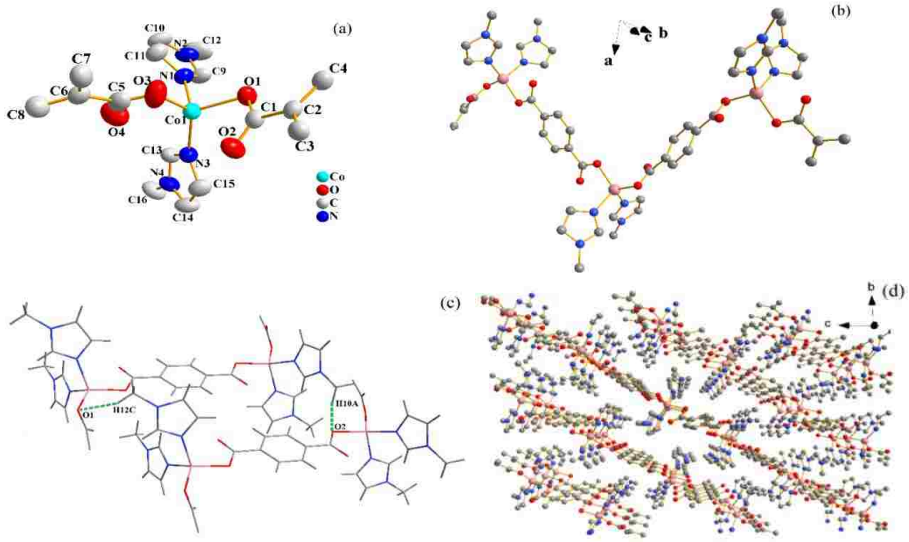

Fig. 3.1. a) Ortep diagram showing the asymmetric unit of 1 with thermal ellipsoid given at 50% probability. Hydrogen atoms are omitted for clarity. b) The zig-zag 1-D Coordination polymer chain. c) Packing Diagram showing 2-D arrangement of the polymeric compound 1 through hydrogen bonds (shown by green dotted line). d) C-H…π induced extensive 3-D network

Nickel forms green 1-D polymeric complex [Ni(BDC)(Mim)$_{2}$]n 2 almost isostructural to 1. The polymer crystallizes in monoclinic C2/c and each Ni(II) atom has a distorted octahedral coordination environment with the terephthalate ligands (BDC) coordinated in a *bis*-bidentate fashion (Fig. 3.2). Two 1,4-BDC units takes on a *cis*-

conformation around the Ni(II) center along with two terminal Mim in out of plane fashion. The BDC ligand acts as a bridge between two Ni(II)-atoms and thereby propagates the zig-zag polymeric chain. The Ni-O bond lengths are between 2.071(2) Å and 2.00(3) Å, and the Ni-N bond lengths are 2.027(3) Å. Such coordination geometry is in accord with an octahedrally coordinated Ni (II) in the high spin state, [18]. The complex shows Ni-Ni bond distance of 10.6295(16) Å and the angle between three consecutive Ni-atoms (Ni-Ni-Ni) is found to be 103.76(1) °

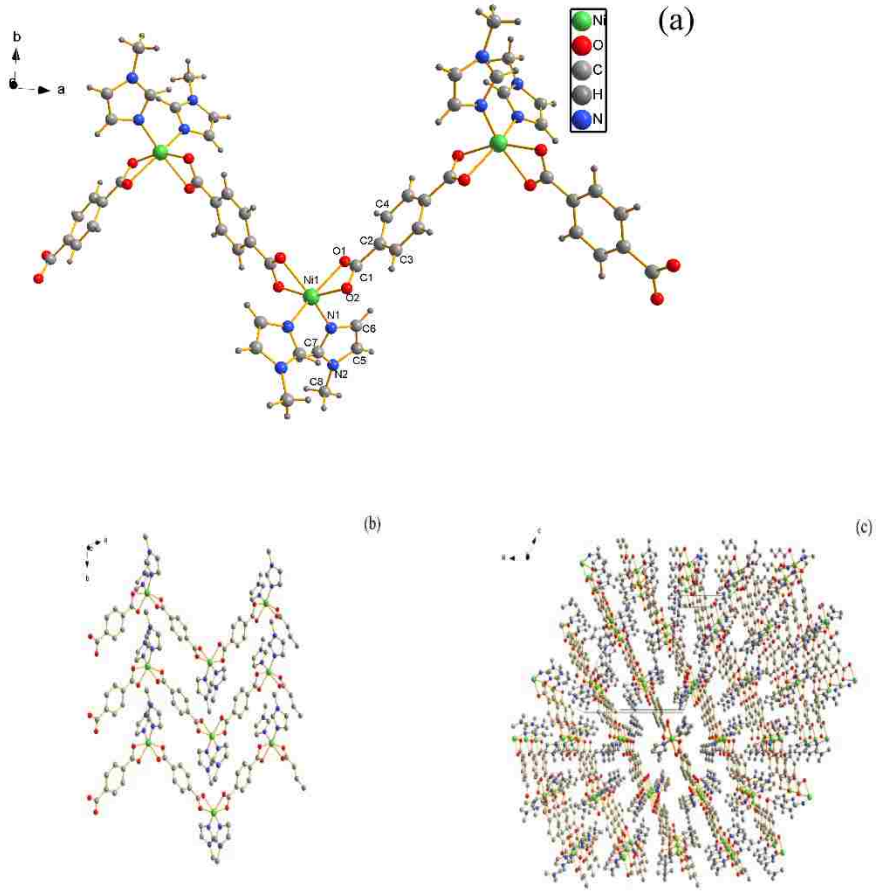

Fig. 3.2. (a) The zig-zag 1D coordination polymer chain of 2. The asymmetric unit of 2 is labelled. (b) Packing diagram showing H-bond stabilized 2-D arrangement of the polymeric compound 2. (c) C-H..π induced extensive 3-D network

The structure packs as infinite chains that extend along c-axis through hydrogen bonding interaction (C(8)-H(8A)..O(2) = 2.49 Å and C(8)-H(8C)..O(1) = 2.37 Å) (Table 2.3, Appendix) from both methyl groups where each methyl group is hydrogen-bonded to two carboxylate oxygen (Fig. 3.2b). Furthermore, the 2-D layers give rise to 3-D supramolecular network (Fig. 3.2c) *via* CH…π interactions (Table 2.4, Appendix) evident from C-H..π distance of 2.75 Å to 3.0 Å. The Cu(II) polymeric complex $[Cu(BDC)(Mim)_2]_n$ (3) crystallizes in monoclinic crystal system with $P2_{(1)/}n$ space group (Fig. 3.3). The Cu(II) center is square planar with two *bis*-monodentate BDC and two terminal Mim in *trans* geometry. The Cu compound forms a linear chain (Cu-Cu-Cu angle is 180°) along "c" direction with two BDC ligands in plane at the axial position and two in plane terminal MIM at the equatorial position, making Cu an inversion center. Table 1 gives the crystallographic data of the complexes. The Cu-O and Cu-N bond lengths are 1.9454(18) Å and 1.993(3) $Å_2$, respectively with Cu-Cu distance of 10.955(3) Å. The 1-D polymeric complex **3** packs as infinite rows and columns in the solid state. The 3-D solid crystalline structure was found to be stabilized by non-covalent π- π, CH… π and H-bonding interaction. Inter-molecular and intramolecular H-bonding interaction is found to be produced by the hydrogens in the Mim unit (Fig. 3.3b).

Hydrogen atoms (H1A and H2A) from C1 and C2 carbon in Mim unit forms intramolecular H-bonding with O1 (2.52-2.53Å) which results in the co-planarity of Mim and O1-O1′ unit (Table 3.3, Appendix). The 2-D framework from the infinite 1-D polymeric chain is formed through intermolecular H-bonding interaction between 02′-H1A (2.53 Å) and 02′-H4A (2.53 Å) along with CH… π interaction between C(4)-H(4C) and Cg(3) (centroid of Mim unit) (2.94 Å) ring (Table 3.4, Appendix).

Table 1. Crystallographic data for 1, 2 and 3.

	$[Co(BDC)(Mim)_2]n$	$[Ni(BDC)(Mim)_2]n$	$[Cu(BDC)(Mim)_2]n$
	1	2	3
Empirical Formula	$C_{16}H_{16}N_4O_4Co$	$C_{16}H_{16}N_4O_4Ni$	$C_{16}H_{16}N_4O_4Cu$
Formula Weight (g/mol)	387.26	387.04	391.87
Wavelength (Å)	0.71073	0.71073	0.71073
Crystal System	Triclinic	Monoclinic	Monoclinic
Space Group	P-$\bar{1}$	C2/c	$P2_{(1)}/n$
a (Å)	7.3256 (7)	17.338 (4)	5.3003 (15)
b (Å)	9.0006 (9)	7.2141 (16)	14.729 (4)
c (Å)	13.7874 (14)	15.562 (4)	10.955 (3)
α (°)	82.0240 (10)	90	90
β (°)	78.2670 (10)	119.316 (3)	102.954
γ (°)	72.3450 (10)	90	90
Volume ($Å^3$)	845.25 (15)	1702.2 (7)	833.5 (4)
Z	2	4	2
Calculated Density (mg/m^3)	1.522	1.51	1.561
Goodness of fit on F^2	1.056	0.973	0.996
Final R indices I>2sigma	R1= 0.0426 wR2= 0.1059	R1= 0.0493, wR2= 0.0931	R1= 0.0433 wR2= 0.0941
R indices (all data)	R1= 0.0503 wR2= 0.1101	R1= 0.0816, wR2= 0.1041	R1= 0.0728 wR2= 0.1060
Largest diff. Peak/`Hole	0.460/ -0.240	0.402/-0.339	0.380/-0.231

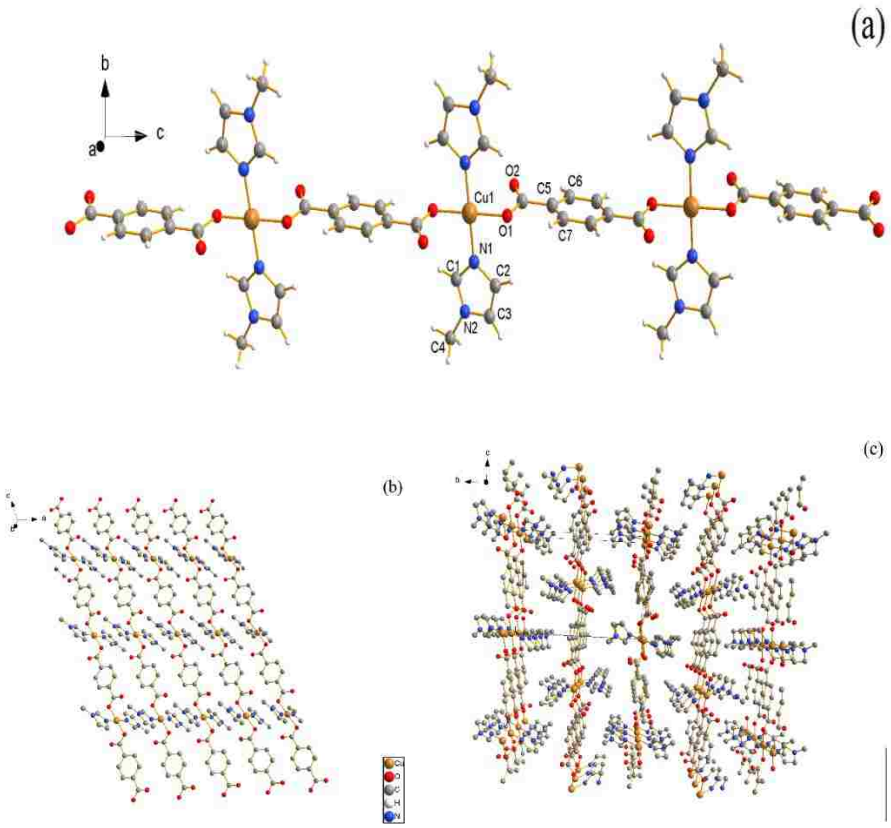

Fig. 3.3. (a) The polymeric 1D coordination chain of 3. The asymmetric unit of 3 is labelled.(b) Packing diagram showing H-bond stabilized 2-D arrangement of the polymeric compound 3. (c) C-H..π induced extensive 3-D network

3.1.2. Powder X-ray Diffraction. After the sample was dried it was well ground using a mortar pestle and the ground sample was subjected to powder X-ray diffraction (PXRD). The PXRD pattern of the as-synthesized sample is plotted against the simulated one in Fig. 3.4(a-c). In all cases, excellent agreement between the simulated and the experimental patterns was found and indicates high bulk purity of the as-synthesized phases.

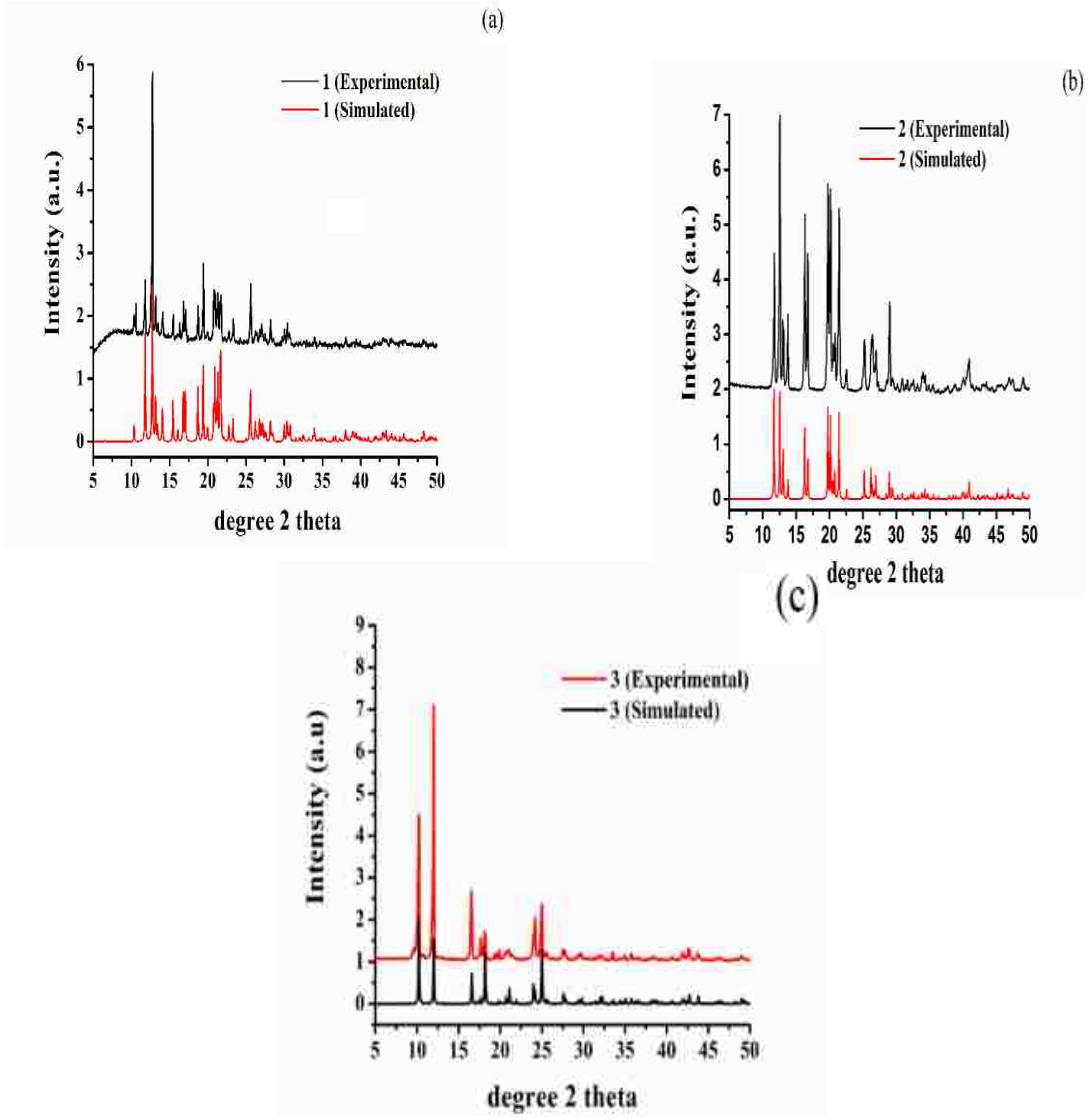

Fig. 3.4. Experimental and simulated PXRD pattern for (a) 1, (b) 2 and (c) 3

3.1.3 FT-IR. In the FT-IR spectrum of 1 (Fig. 3.5), the coordination of carboxylic group to the metal center is evident from the change of υ(C=O) bands to lower wavelength, from 1720 cm^{-1} in BDC to 1588 cm^{-1} in the coordination polymer, [17, 19]. The respective υ(C=O) bands for 2 and 3 were found at 1603 and 1560 cm^{-1}, respectively. The presence of Mim unit was also evident through characteristic peaks at 2963 cm^{-1}, 1425 cm^{-1} and

1360 cm^{-1}, known for coordinated Mim, [19]. The peaks associated for Mim unit in 2 was found at1428, 2950 and 3137 and at 1417, 2963, and 3130 for 3.

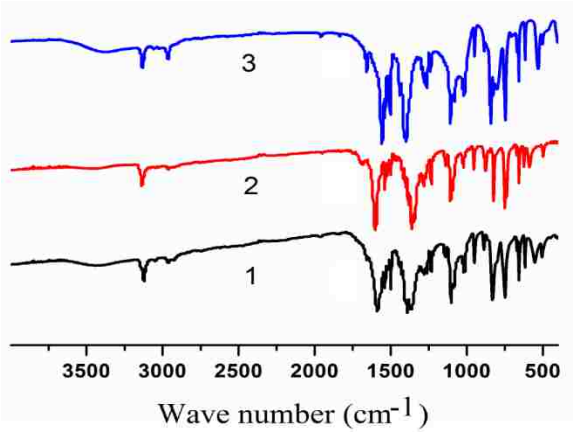

Peaks	1	2	3
$\upsilon_{(C2\text{-}N1\text{-}C5)}$ Imidazole bending	652	654	658
Out of plane $\upsilon_{(C\text{-}H)}$ bending of imidazole ring	739	748	746
In plane imidazole ring breaking	834	825	841
$\upsilon_{(C\text{-}H)}$ Imidazole ring	1425	1428	1417
$\upsilon_{(C=O)}$ carboxylic acid	1588	1603	1560
$\upsilon_{(C\text{-}H)}$ Imidazole ring	2963	2950	2960
$\upsilon_{(C\text{-}H)}$ Imidazole ring	3125	3137	3130

Fig. 3.5. FT-IR spectra of 1, 2 and 3 in KBr disc

3.1.4. Thermo-Gravimetric Analysis. The polymeric complexes 1, 2 and 3 were subjected to thermogravimetric analysis (TGA). TGA thermogram of 1 reveals loss of 22 wt. % around 200^{o}C and almost 42% at a temperature of 400^{o}C (Fig. 3.6). The weight losses accounts for the step wise removal of two Mim units between 180^{o}- 400^{o}C and almost complete decomposition of 1,4-BDC moiety at a temperature of 550^{o}C. The final weight loss at around 550° C accounts for ~77 wt. % of total weight loss. According to elemental calculation ($C_{16}H_{16}N_4O_4Co$), the final weight (~23%) is higher than that expected for just metallic cobalt (~15%) which shows interesting thermal induced modification.

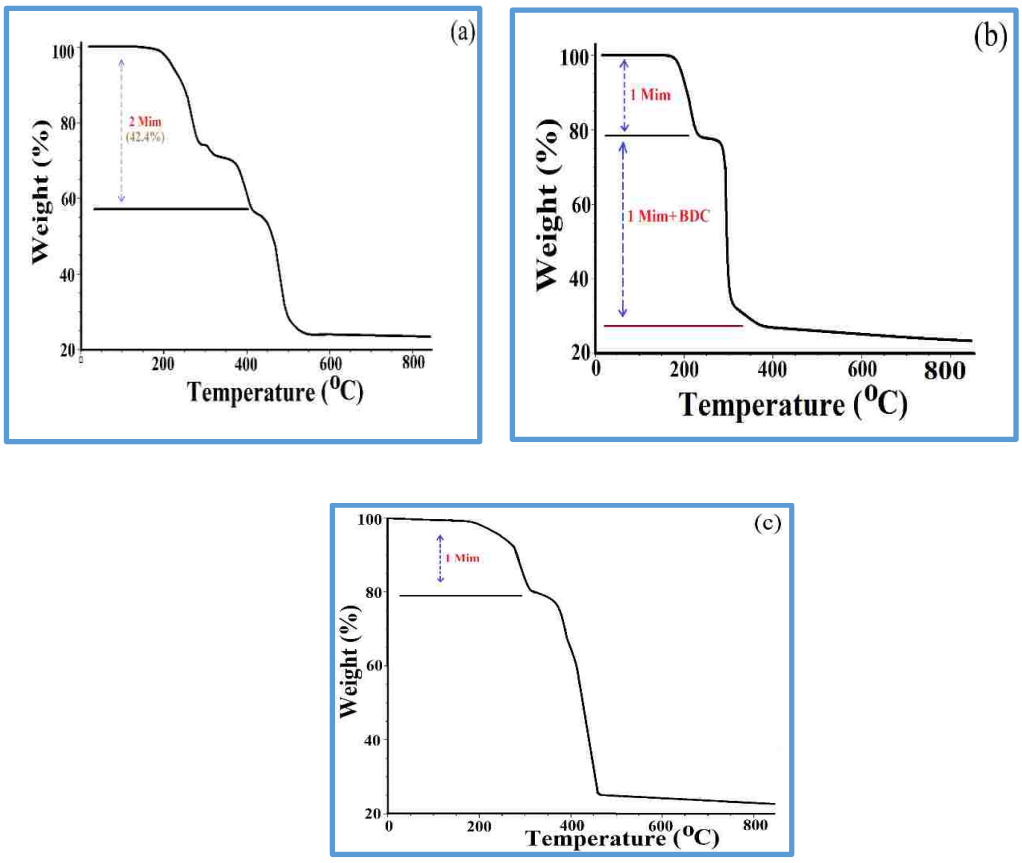

Fig. 3.6. TGA thermogram of (a) 1, (b) 2 and (c) 3 under N_2

TGA of polymeric nickel complex 2 shows the complete removal of one Mim unit at around 200°C and accounts for ~22% weight loss. The second and final weight loss (53%) was seen at around 300°C which may be due to complete loss of Mim unit and the decomposition of BDC unit. Similar to the TGA profile of 1, the final product of 2 also showed the presence of byproduct of pyrolysis. Furthermore, TGA of 3 also showed similar thermal profile with Mim unit decomposing in two increments between 200-300°C and 380- 450°C. Analogous to 1 and 2, 3 also shows the presence of some additional weight not accounted for metal particle.

4. THERMAL DECOMPOSITION

4.1 PYROLYSIS OF 1

Preliminary TGA results indicated chemical modification of 1, 2 and 3 on heating. Driven by this observation, the polymeric complex 1, 2 and 3 was then subjected to controlled pyrolysis under N_2 in a CVD furnace. In case of 1, the synthesis was optimized at 550^{o}C and a dark carbonaceous solid Co@C_550 was formed.

4.1.1. PXRD. The PXRD of Co@C_550 reveals the formation of metallic *fcc* cobalt (Co^0) phase (Fig. 4.1a), [20]. A plot of the PXRD of as-synthesized Co@C phases through the decomposition of 1 at different temperature is given in Fig. 4.1b indicating the evolution of *fcc* cobalt phase at 550^{o}C, [20].

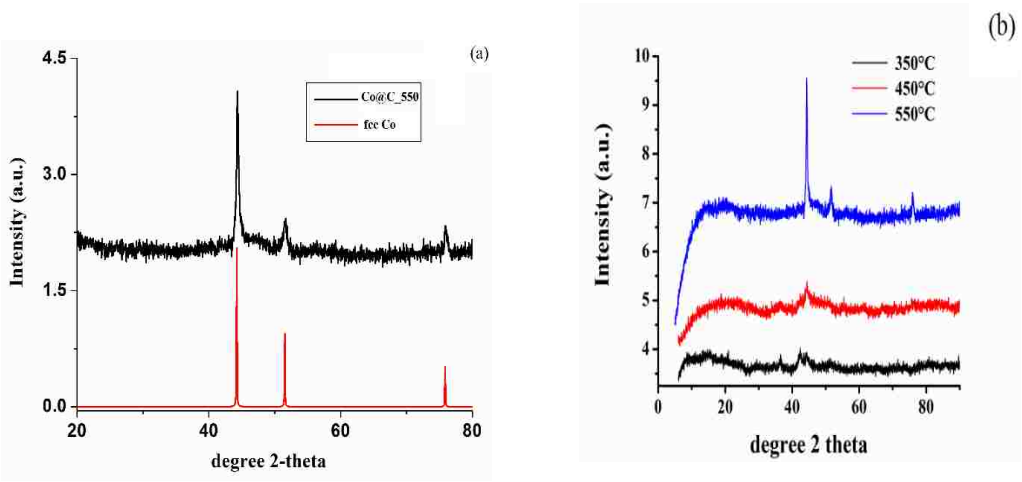

Fig. 4.1. (a) PXRD pattern of as synthesized Co@C_550 (top, black line) is shown against literature reported[20] (bottom, red line). (b) PXRD pattern for the pyrolysis of 1 at different temperature under N_2

It is to be noted that Co@C_550 is devoid of any conventional carbides of Co such as Co_2C and Co_3C, and may be due to lower decomposition temperature of Co_2C (300^{o}C)

and Co_3C (315°C), [21]. Elemental analysis of Co@C_550 prepared through five independent syntheses supports TGA results with presence of carbon percentage between 35.07% - 35.36%, showing bulk carbonization of Co@C_550. The carbonization route via decomposition of 1-D analogue was found to be quite interesting and provides ample opportunity for fine tuning of the products. For example, when 1 was initially heated at 300°C under N_2 for 2 h and then at 550° C for 2 h under forming gas (95% N_2 and 5% H_2), tricobaltetraoxide (Co_3O_4) phases was formed (Fig. 4.2), [22].

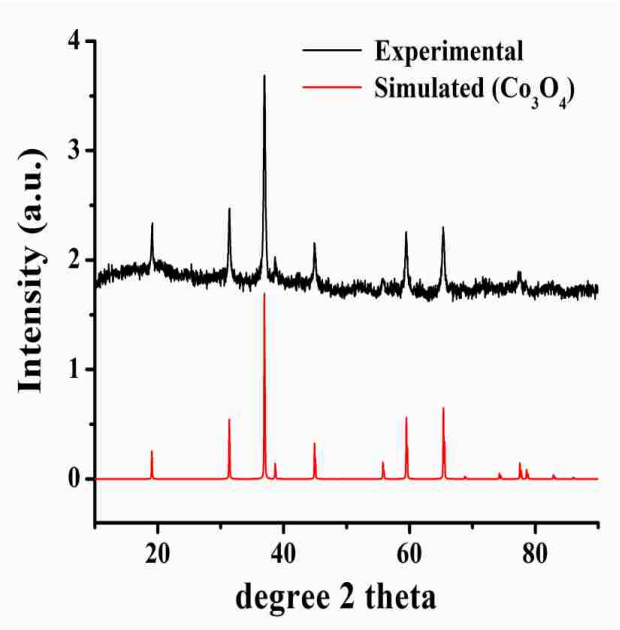

Fig. 4.2. PXRD pattern of the decomposition of 1 at 550°C under forming gas showing the formation of Co_3O_4 phase

4.1.2. SEM. SEM image shows aggregated near spherical carbonaceous metal clusters distributed in the size range of 200-500nm (Fig. 4.3a). Physical magnetic separation of a suspension of 2 in EtOH allows almost quantitative collection of the solid in the vicinity of the magnet within 2 min (Fig. 4.3b-4.3c) which strongly implies the presence of carbon coated magnetic metal particles.

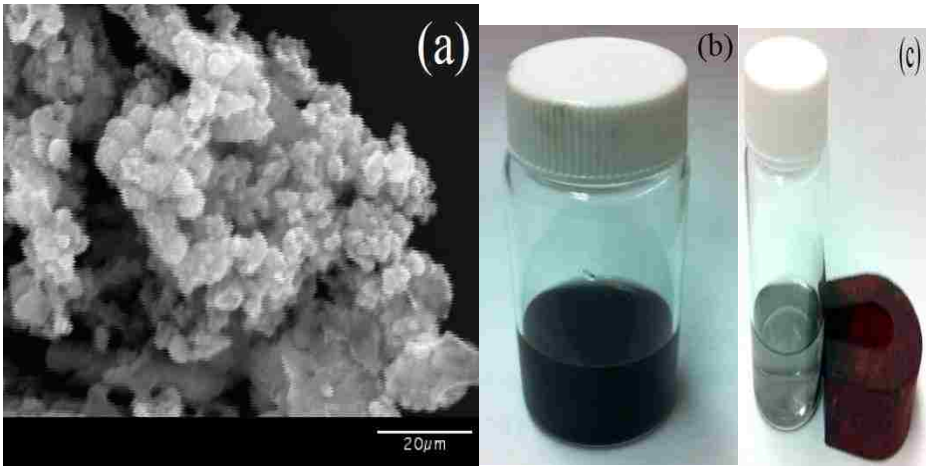

Fig. 4.3. (a) SEM image of as synthesized Co@C_550 collected with Au sputtering. (b) Physical suspension of Co@C_550 in ethanol being (c) separated by a horse shoe magnet

4.1.3. TEM Measurements. STEM image shows cobalt particles of 20-100 nm size highly embedded in a carbon matrix (Fig. 4.4a). This is supported by line mapping over a region of 400 nm (Fig. 4.4b) across the metal nanoparticles. Based on the mass contrast as shown in (Fig. 4.4c) on a single cobalt nanoparticle, the light domain is carbon rich and the dark domain is cobalt rich. The dark domain is highly crystalline while the boundaries are amorphous. SAED pattern on dark domain shows highly crystalline *fcc* cobalt (Fig. 4.4d) while the HRTEM micrographs showed the presence of graphitic carbon shell along cobalt particles evident from analysis of the lattice fringes with d-spacing of 0.34 nm, [23].

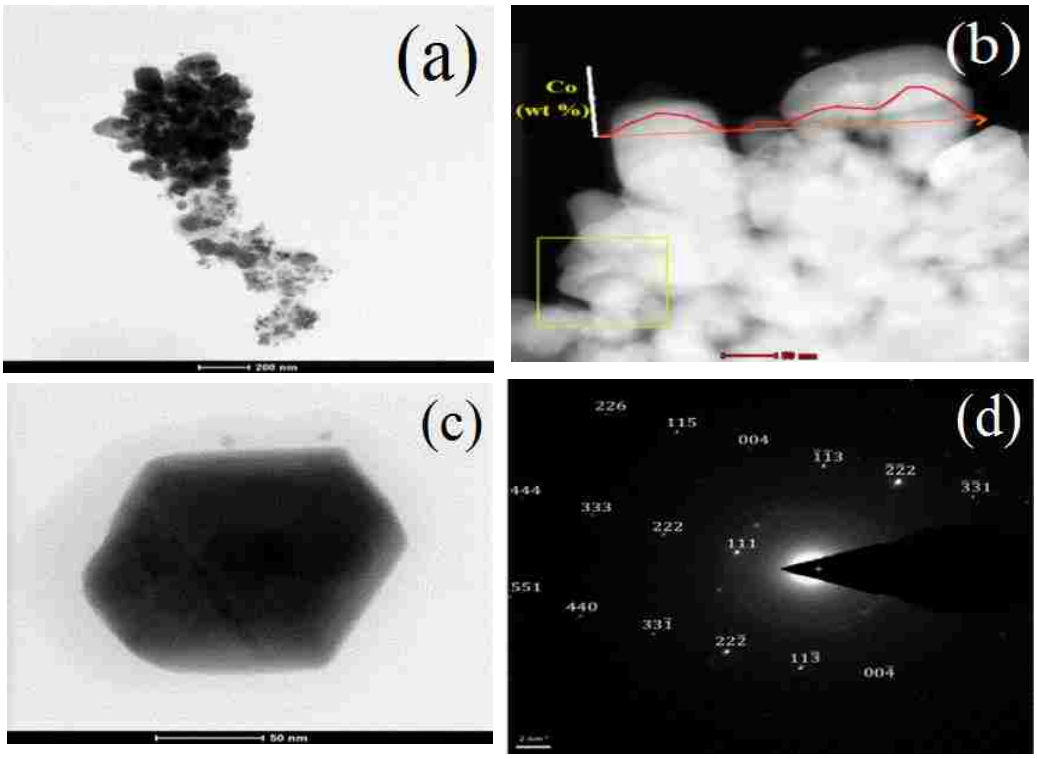

Fig. 4.4. (a) STEM image of as synthesized Co@C_550 (b) Line mapping of Co@C_550 over a range of 400 nm showing the variation of wt % of Co over the distance(orange line). The yellow box is for reference. (c) STEM image of a single Co nanoparticle and its (d) electron diffraction pattern indexed to cubic cobalt; viewed along [$\bar{1}$11] zone axis

4.1.4. Raman and XPS. The presence of carbon coating is further supported by Raman scattering experiment of Co@C_550 which shows two bands at 1364 cm^{-1} and 1587 cm^{-1} (Fig. 4.5a) assigned to D and G bands of disordered and graphitic carbon respectively, [24]. Furthermore, XPS of Co@C_550 (Fig. 4.5b) done without Ar sputtering gives Co $2p_{3/2}$ peak at 778.3 eV characteristic of zero-valent metallic cobalt, [25]. However, peak at 781.3 eV along with shake up satellite peaks for Co(II) species was also found. Since PXRD excludes the possibility of Co(II) species, the observed Co(II) indicates oxidation of reactive metallic cobalt surface to CoO through slow oxidation in air which has been observed previously, [26].

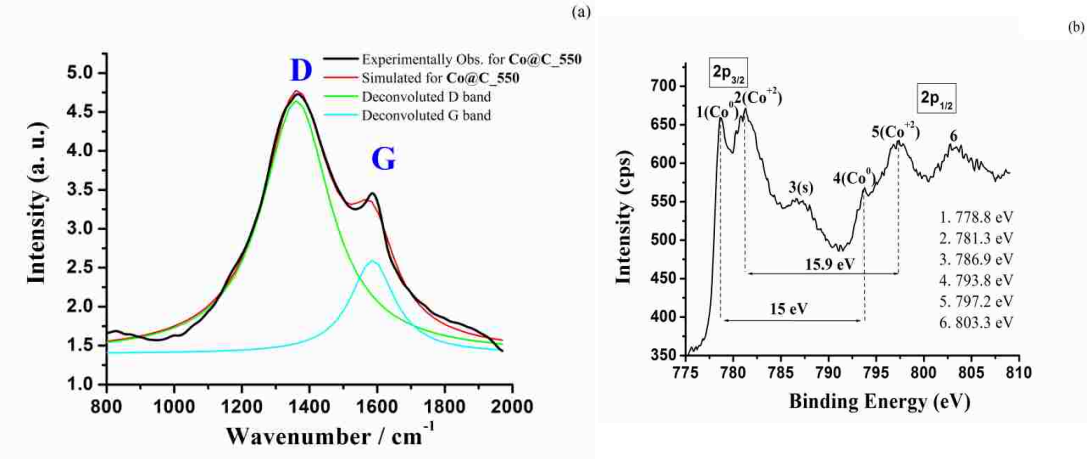

Fig. 4.5. Raman spectra for Co@C_550 designating the D (1364 cm^{-1}) and G(1587 cm^{-1}) band (I_G/I_D=0.37). (b) Cobalt 2p XPS spectrum of Co@C_550 without Ar sputtering. Peaks assigned are listed numerically in the inset. Metallic cobalt (Co^0), divalent cobalt (Co^{+2}), and Co^{+2} shake-up satellites (s) are labelled. Co^{+2} peaks are noted to have formed from slow oxidation of reactive metallic cobalt with oxygen

4.2. PYROLYSIS OF 2.

Similarly the polymeric nickel complex 2 was also subjected to pyrolysis which gives a carbonaceous product Ni@C (Fig. 4.6a), a mixture of Ni_3C and *fcc* Ni, [21, 27]. The plot of the PXRD of as-synthesized Ni@C phases at different temperature is given in Fig. 4.6b and shows the decomposition of 2 at temperature above 250°C and the evolution of Ni@C phases.

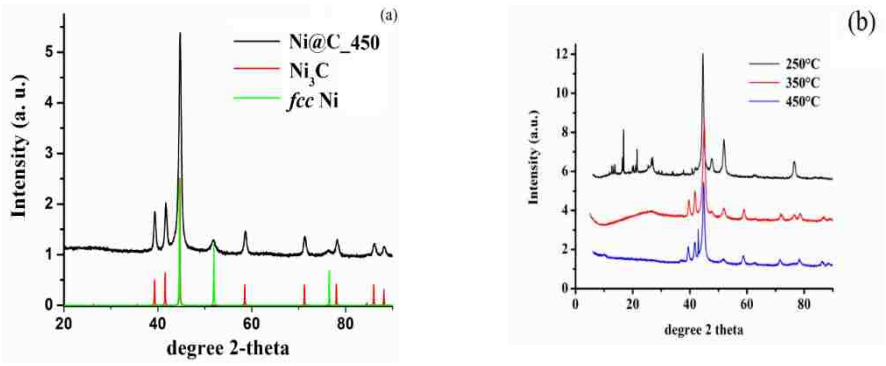

Fig. 4.6. (a) PXRD pattern of as synthesized Ni@C_450 (top, black line) is shown against literature reported for *fcc* Ni[21] and Ni_3C[27] (red & green line). (b) PXRD pattern for the pyrolysis of 2 at different temperature under N_2

4.2.1. Surface Area Study of NI@C. The nickel complex 2 after pyrolysis is subjected to surface area study to check the surface area which is an important factor in determining the catalytic activity. The surface area study is done using Brunauer-Emmett-Teller isotherm. Fig. 4.7 shows the surface area and the pore volume of the material the sample Ni@C_450 was found to have a surface area of 126.39 m^2/g and a pore volume of 0.7612 cc/g. The adsorption isotherm that is formed is type 2 adsorption isotherm and intermediate layer is due to monolayer formation.

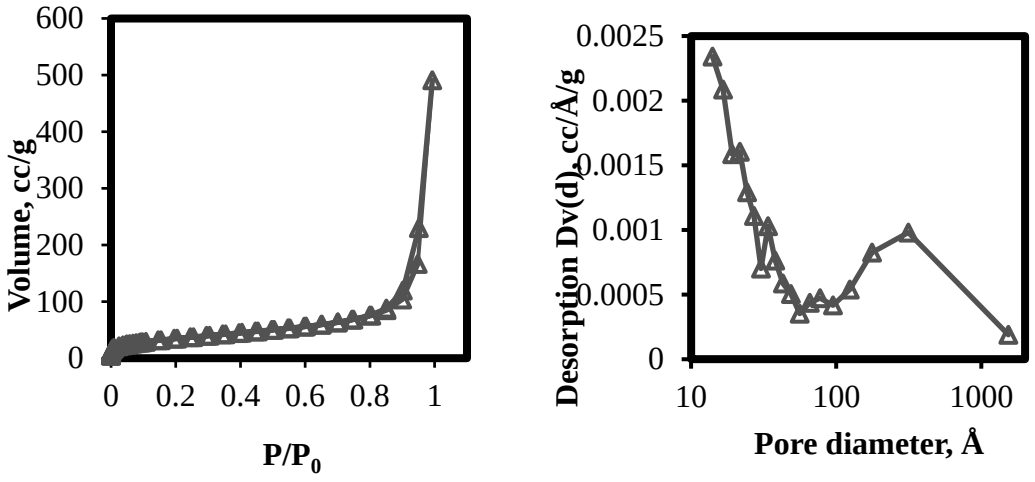

Fig. 4.7. (a) BET Isotherm and (b) Pore size distribution of Ni@C_450

4.3. PYROLYSIS OF 3

Similar to 1 and 2, 3 also gives carbonized metal particles on pyrolysis. The decomposition of 3 gives dark carbonaceous Cu@C solid and PXRD shows the formation of *fcc* copper particles at 450°C under N_2 (Fig. 4.8a), [28]. The plot of the PXRD of as-synthesized Cu@C phases at different temperature is given in Fig. 4.8b and shows the decomposition of 3 at temperature above 250°C.

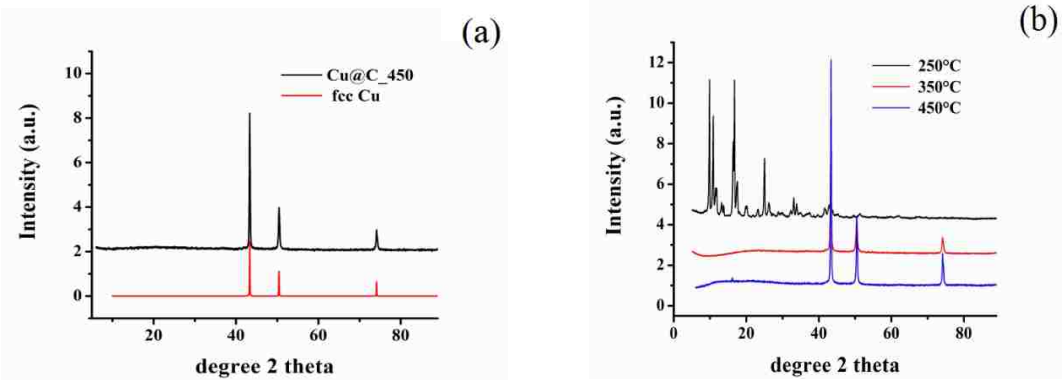

Fig. 4.8. (a) PXRD pattern of as synthesized Cu@C_450 (top, black line) is shown against literature reported for *fcc* Cu[28] (bottom, red line). (b) PXRD pattern for the pyrolysis of 3 at different temperature under N_2

This shows that these 1-D polymeric complexes based on BDC and Mim are a good precursor for carbonization of metal particles and the route to carbonization of metal particle is indeed general.

5. CATALYTIC STUDY

The suitability of Co@C and Ni@C as a catalyst was evaluated as cobalt and nickel particles are very well known for catalytic application. As a model reaction, the hydrogenation of para-nitrophenol (PNP) to para-aminophenol (PAP) at room temperature was performed to test the catalytic activity of the as-synthesized carbonized metal particles. PNP and other nitro phenols derivatives are common byproducts of pesticides, herbicides, and synthetic dyes production and the reaction is a strong indicator for catalytic potential, [29].

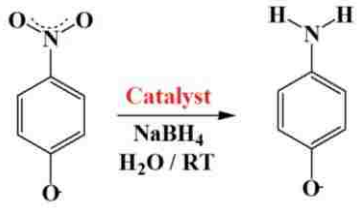

Scheme 1: Schematic presentation of conversion of PNP to PAP

Preliminary reaction of PNP with 5 mol % of Co@C_550 using 20 eq. $NaBH_4$ (Co@C: PNP: $NaBH_4$ = 1:20:400) in H_2O at room temperature gave quantitative conversion to PAP. For comparison, identical reaction without Co@C_550 (blank) or with 1 shows almost no or negligible PNP conversion which indicates the indispensable role of Co@C_550 for the conversion. Fig. 5.1 shows the reduction of PNP through the decrease in absorbance at 400 nm and the generation of PAP at 300 nm. Under identical condition, reaction with Ni@C_450 gave only a yield of 32%. Furthermore, kinetic measurements were performed by monitoring the decrease in absorbance at 400 nm with a molar ratio of 2: PNP: $NaBH_4$ = $1:10^2:10^5$ (catalyst=0.375 μM), [29-31]. Fig. 5.2 (Inset) depicts

negligible change in absorbance at 400 nm in the absence of catalyst (blank). On the other hand, upon addition of **2**, a certain period of time was required for the reaction to start and as inferred earlier, indicates the time required for the PNP to adsorb on the surface of the catalyst, [29]. Under limiting $NaBH_4$ concentration, pseudo-first order kinetics with respect to PNP is applied to the kinetic data, [29, 30].

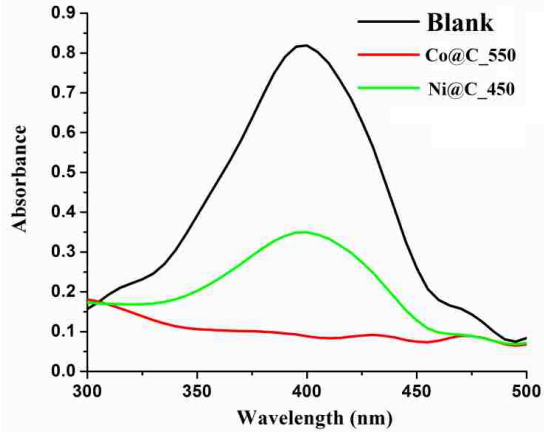

Fig. 5.1. Reduction of PNP to PAP with Co@C_550 (red line), Ni@C_450 (green line) and in absence of any catalyst (black line)

The slope of near linear fit plot of the natural log of absorbance at 400 nm versus time (inset, Fig. 5.2, red line) gives the apparent rate constant [30], (K_{app}= 0.31 ± 0.02 min^{-1}). Under the given reaction condition, the induction period or the average time of absorbance (t_{ads}) = 1.6 minutes for three independent kinetic measurements and implies the time required for the reaction to occur on the surface of the catalyst, [29]. This shows the adsorption is indeed playing a major role in the catalytic process and on the catalytic activity of Co@C_550.

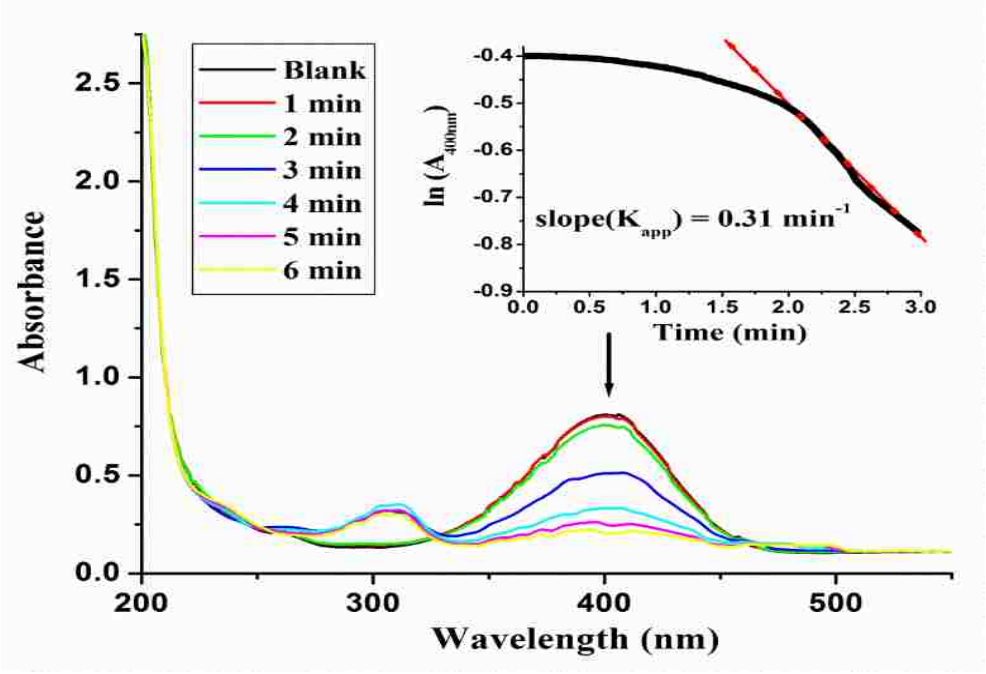

Fig. 5.2. Catalytic reduction of PNP using Co@C_550 studied by uv-vis with increment of time. Inset: Plot of natural log of absorbance vs time showing the apparent rate constant marked by red line

6. CONCLUSION

In summary, the work presents an easy pathway for the generation of carbon coated metal particles through reduction of polymeric 1-D coordination polymer. The facile reduction of PNP to PAP using $NaBH_4$ with Co@C shows the active nature of the material. The presence of catalytically active metallic particle with strong adsorption property, evident through the adsorption of PNP on the surface of Co@C, makes it a promising candidate for use in LT Fisher Tropsch synthesis (FTS)[20]. The absence of conventional Co(II) carbides, known to be responsible for deactivation process in FTS [32], further adds up its suitability as a catalyst for the reaction.

APPENDIX

Table 1.1. Atomic Coordinates and equivalent isotropic displacement parameters/$Å^2$ for 1

Atom	x	Y	z	U (eq)
Co(1)	1957(1)	7914(1)	7696(1)	42(1)
O(1)	168(2)	8398(2)	8996(1)	51(1)
O(2)	-1155(3)	10083(2)	7841(1)	61(1)
C(1)	-1278(4)	9421(3)	8689(2)	45(1)
C(2)	-3201(3)	9746(3)	9378(2)	41(1)
C(3)	-4897(3)	10507(3)	9003(2)	43(1)
C(4)	-3312(3)	9245(3)	10382(2)	45(1)
O(3)	504(4)	6790(3)	7113(2)	79(1)
O(4)	3193(4)	6579(3)	6043(2)	92(1)
C(5)	1552(5)	6376(3)	6303(2)	61(1)
C(6)	744(4)	5644(3)	5634(2)	48(1)
C(7)	-1017(4)	5330(3)	5938(2)	54(1)
C(8)	1768(4)	5308(3)	4695(2)	55(1)
N(1)	4217(3)	6186(2)	8191(2)	49(1)
C(9)	5457(5)	6345(3)	8700(2)	60(1)
N(2)	6847(3)	5008(3)	8823(2)	62(1)
C(10)	6469(5)	3930(4)	8358(3)	72(1)
C(11)	4856(4)	4658(3)	7973(2)	62(1)
C(12)	8509(6)	4811(5)	9320(3)	101(2)
N(3)	3321(3)	9527(2)	7009(2)	46(1)
C(13)	5190(4)	9169(3)	6637(2)	53(1)
N(4)	5718(3)	10384(3)	6137(2)	54(1)
C(14)	4096(5)	11608(4)	6189(2)	65(1)
C(15)	2626(4)	11083(3)	6728(2)	59(1)
C(16)	7704(5)	10371(5)	5650(2)	74(1)

Table 1.2. Selected bond lengths (Å) and bond angles (°) for 1

Co(1)-O(3)	2.007(2)	Co(1)-N(3)	2.029(2)
Co(1)-O(1)	2.0083(18)	Co(1)-N(1)	2.056(2)
O(3)-Co(1)-O(1)	99.98(9)	O(3)-Co(1)-O(1)	99.98(9)
O(3)-Co(1)-N(3)	128.46(10)	O(3)-Co(1)-N(3)	128.46(10)
O(1)-Co(1)-N(3)	117.77(8)	O(3)-Co(1)-N(3)	117.78(8)

Table 1.3. Non-covalent H-bonding interaction in 1-D Co-Polymeric complex 1

H-bonding Interaction in 1			
D-H…A	d(H…A) Å	D-H…A.angle (o)	Symmetry code
C(10)-H(10A)..O(2)	2.56	167	[1465.01]
C(12)-H(12C)..O(1)	2.55	160	[2665.01]
D-H…A= Donor-Hydrogen…Acceptor; [1465] =1-x,1-y,-z; [2665] =- 1+x,1+y,z.			

Table 1.4. Non-covalent CH… π interaction in 1-D Co-Polymeric complex 1

CH… π Interaction in 1			
X-H…Cg(J)	d(H….Cg) Å	γ-angle (o)	Symmetry code
C(7)-H(7A)…Cg(3)	2.93	9.24	[1655.01]
C(3) -H(3A)…Cg(4)	2.84	5.01	[1655.01]
C(9)-H(9A)…Cg(5)	2.93	18.53	[1455.01]
Cg(J) = center of gravity of ring J; γ-angle = angle between Cg-H vector and ring normal. Centroid: Cg(3) =N(1)-C(9)-N(2)-C(10)-C(11), Cg(4) = N(3)-C(13)-N(4)-C(14)-C(15), Cg(5) = C(2)-C(3)-C(4)b-C(2)b-C(3)b-C(4). [1455] = -1+x,y,x; [1655] = 1+x,y,z.			

Table 2.1. Atomic coordinates and equivalent isotropic displacement parameters/$Å^2$ for 2

Atom	x	y	z	U (eq)
Ni(1)	5000	7954(1)	7500	39(1)
O(1)	5922(2)	10208(4)	7691(2)	57(1)
O(2)	6022(2)	8516(3)	8903(2)	49(1)
C(1)	6257(2)	9902(5)	8592(3)	41(1)
C(2)	6911(2)	11228(5)	9318(3)	39(1)
C(3)	7343(2)	10826(6)	10314(3)	46(1)
C(4)	7074(2)	12919(6)	9004(3)	46(1)
C(5)	3630(3)	4875(7)	8610(4)	75(2)
C(6)	3680(3)	6313(7)	8082(4)	64(1)
N(1)	4412(2)	6110(4)	7977(2)	42(1)
C(7)	4783(3)	4570(5)	8451(3)	46(1)
N(2)	4330(2)	3774(5)	8841(2)	54(1)
C(8)	4557(4)	2028(7)	9384(4)	85(2)

Table 2.2. Non-covalent H-bonding interaction in 1-D Ni-Polymeric complex 2

H-bonding Interaction in **2**			
D-H…A	d(H…A) Å	D-H…A angle (°)	Symmetry code
C(8)-H(8A)..O(2)	2.49	142	-x+1, -y+1, -z+2
C(8)-H(8C)..O(1)	2.37	144	-x+1, y-1, -z+3/2

Table 2.3. Selected bond lengths (Å) and bond angles (°) for 2

Ni(1)-N(1)	2.027(3)	Ni(1)-O(2)[b]	2.071(2)
Ni(1)-N(1)[b]	2.027(3)	Ni(1)-O(1)	2.200(3)
Ni(1)-O(2)	2.071(3)	Ni(1)-O(1)[b]	2.200(3)
N(1)-Ni(1)-N(1)[b]	97.97(17)	O(1)-Ni(1)O(1)[b]	84.67(15)
N(1)-Ni(1)-O(2)	93.93(11)	N(1)-Ni(1-C(1)	124.10(12)
N(1)[b]-Ni(1)-O(2)	100.85(11)	N(1)[b]-Ni(1)-C(1)	101.08(12)
N(1)-Ni(1)-O(2)[b]	100.85(11)	O(2)-Ni(1)-C(1)	31.00(11)
N(1)[b]-Ni(1)-O(2)[b]	93.93(11)	O(2)[b] -Ni(1)-C(1)	129.25(12)
O(2)-Ni(1)-O(2)[b]	157.43(15)	O(1)-Ni(1)-C(1)	30.53(10)
N(1)-Ni(1)-O(1)	154.27(11)	O(1)[b]-Ni(1)-C(1)	90.76(12)
N(1)[b]-Ni(1)-O(1)	93.98(12)	N(1)-Ni(1)-C(1)[b]	101.08(12)
O(2)-Ni(1)-O(1)	61.34(10)	N(1)[b]-Ni(1)-C(1)[b]	124.10(12)
O(2)[b]-Ni(1)-O(1)	100.97(10)	O(2)-Ni(1)-C(1)[b]	129.25(12)
N(1)-Ni(1)-O(1)[a]	93.98(11)	O(2)[b] -Ni(1)-(1)[b]	31.00(11)
N(1)[b]-Ni(1)-O(1)[b]	154.27(11)	O(1)-Ni(1)-C(1)[b]	90.76(12)
O(2)-Ni(1)-O(1)[b]	100.97(10)	O(1)[b]-Ni(1)-C(1)[b]	30.53(10)
O(2)[b]-Ni(1)-O(1)[b]	61.34(10)	C(1)-Ni(1)-C(1)[b]	109.99(18)

[a] Symmetry transformations used to generate equivalent atoms

[b] -x+1, y, -z+3/2

Table 2.4. Non-covalent CH… π nteraction in 1-D Ni-Polymeric complex 2

CH… π Interaction in **2**			
X-H…Cg(J)	d(H….Cg) Å	γ-angle (°)	Symmetry code
C(4)-H(4A)…Cg(1)	2.75	1.28	[2645.01]
C(8)-H(8A)…Cg(1)	3.00	13.25	[3665.01]
Cg(J) = center of gravity of ring J; γ-angle = angle betwee Cg-H vector and ring J normal. Centroid: Cg(1) =N(1)-C(6)-C(5)-N(2)-C(7) [2645] = 1-x,-1+y,1/2-z; [3665] = 1-x,1-y,-z.			

Table 3.1. Atomic coordinates and equivalent isotropic displacement parameters/$Å^2$ for 3

Atom	x	y	Z	U (eq)
Cu(1)	0	5000	5000	40(1)
O(1)	868(4)	5165(1)	3380(2)	48(1)
O(2)	-2241(5)	4154(2)	2730(3)	57(1)
C(5)	-605(6)	4696(2)	2543(2)	41(1)
C(6)	-257(6)	5348(2)	1220(2)	36(1)
C(7)	1812(6)	5348 (2)	1004(2)	42(1)
C(8)	2060(6)	5498 (2)	-205(2)	41(1)
N(2)	5438(5)	2972 (2)	5217(2)	52(1)
C(1)	4142(6)	3698(2)	4716(3)	47(1)
N(1)	2594(5)	4004(2)	5414(2)	45(1)
C(2)	2950(7)	3428(4)	6421(3)	59(1)
C(3)	4678(8)	2791(2)	6305(3)	65(1)
C(4)	7243(8)	2431(3)	4679(4)	75(1)

Table 3.2. Selected bond lengths (Å) and bond angles (º) for 3

Cu(1)-O(1)^b	1.9454(18)	Cu(1)-N(1)^b	1.993(3)
Cu(1)-O(1)	1.9454(18)	Cu(1)-N(1)	1.993(3)
O(1)^b-Cu(1)-O(1)	180.000(1)	O(1)^b-Cu(1)-O(1)	180.000(1)
O(1)^b-Cu(1)-N(1)^b	90.45(9)	O(1)^b-Cu(1)-N(1)^b	90.45(9)
O(1)-Cu(1)-N(1)^b	89.55(9)	O(1)-Cu(1)-N(1)^b	89.55(9)

^{b} -x, -y+1, -z

Table 3.3. Non-covalent π- π interaction in 1-D Cu-Polymeric complex 3

π- π Interaction in **3**			
Cg(I)…Cg(J)	d(Cg…Cg) Å	β-angle (º)	Symmetry code
Cg(1)…Cg(3)	3.5974(10)	29.1	[1555.01]
Cg(1)…Cg(3)	3.5989(10)	28.7	[3566.01]
Cg(2)…Cg(3)	3.5989(10)	28.7	[1555.01]
Cg(2)…Cg(3)	3.5974(10)	29.1	[3566.01]
β-angle = angle between Cg(I)-Cg(J) or Cg(I)-->Me vector and normal to plane I. Centroid: Cg(1) =Cu(1)-O(1)-C(5)-O(2), Cg(2) = Cu(1)-O(1)b-C(5)b-(O2)b, Cg(3) = N(1)-C(1)-N(2)-C(3)-C(2). [1555] = x,y,x; [3566] = -x,1-y,1-z.			

Table 3.4. Non-covalent CH… π interaction in 1-D Cu-Polymeric complex 3

CH… π Interaction in 3			
X-H…Cg(J)	d(H….Cg) Å	γ-angle (°)	Symmetry code
C(1)-H(1A)…Cg(1)	2.74	22.34	[1555.01]
C(1) -H(1A)…Cg(2)	2.74	22.34	[3566.01]
C(2)-H(2A)…Cg(1)	2.76	24.96	[3566.01]
C(2)-H(2A)…Cg(2)	2.76	24.96	[1555.01]
C(4)-H(4B)…Cg(4)	2.90	17.99	[2545.01]
C(4)-H(4B)…Cg(4)	2.90	17.99	[4555.01]
C(4)-H(4C)…Cg(3)	2.98	25.92	[1655.01]
Cg(J) = center of gravity of ring J; γ-angle = angle betwen Cg-H vector and ring J normal. Centroid: Cg(1) =Cu(1)-O(1)-C(5)-O(2), Cg(2) = Cu(1)-O(1)b-C(5)b-(O2)b, Cg(3) = N(1)-C(1)-N(2)-C(3)-C(2). Cg(4) = C(6)-C(7)-C(8)b-C(6)a-C(7)a. [1555] = x,y,x; [3566] = -x,1-y,1-z; [2545] = 1/2-x,-1/2+y,1/2-z: [4555] = 1/2+x,1/2-y,1/2+z; [1655] = 1+x,y,z.			

Table 3.5. Non-covalent H-bonding interaction in 1-D Cu-Polymeric complex 3

H-bonding Interaction in 3			
D-H…A	d(H…A) Å	D-H…A angle (°)	Symmetry code
C(1)-H(1A)..O(1)a (intra)	2.52	108	[3566.01]
C(1)-H(1A)..O(2)’	2.53	138	[1655.01]
C(2)-H(2A)..O(1)b (intra)	2.53	107	[3566.01]
C(4)-H(4A)..O(2)	2.53	146	[1655.01]
D-H…A= Donor-Hydrogen…Acceptor; [3566] = -x,1-y,1-z; [1655] = 1+x,y,z.			

REFERENCES

1) (a) H. B. Wu, B. Y. Xia, L. Yu, X. Y. Yu and X. W. Lou, Nature Commun.,2015, **6**, 6512(1-8). (b) H. L. Jiang, B. Liu, Y. Q. Lan, K. Kuratani, T. Akita, H. Shioyama, F. Zong and Q. Xu, J. Am. Chem. Soc., 2011, **133**, 11854–11857. (c) W. Chaikittisilp, N. L. Torad, C. Li, M. Imura, N. Suzuki, S. Ishihara, K. Ariga and Y. Yamauchi, Chem. Eur. J., 2014, **20**, 4217–4221.

2) N. L. Torad , M. Hu, S. Ishihara, H. Sukegawa, A. A. Belik, M. Imura, K. Ariga, Y. Sakka and Y. Yamauchi, Small, 2014, **10**, 2096–2107.

3) H. B. Wu, S. Wei, L. Zhang, R. Xu, H. H. Hng and X. W. Lou, Chem. Eur. J. 2013, **19**, 10804–10808.

4) N. L. Torad, M. Hu, Y. Kamachi, K. Takai, M. Imura, M. Naitoa and Y. Yamauchi, Chem. Commun., 2013, **49**, 2521–2523.

5) (a) C. Janiak, Dalton Trans., 2003, 2781-2804. (b) W. L. Leong and J. J. Vittal, Chem Rev., 2011, **111**, 688-764.

6) (a) N. W. Ockwig, O. D. Friedrichs, M. O'Keeffe and O. M. Yaghi, Acc. Chem. Res., 2005, **38**, 176-182. (b) S. Kitagawa, R. Kitaura, Rand S. Noro, Angew. Chem., Int. Ed. 2004, **43**, 2334–2375.

7) T. R. Cook, Y. R. Zheng and P. J. Stang, Chem. Rev., 2013, **113**, 734−777.

8) (a) Y. Hou, T. Huang, Z. Wen, S. Mao, S. Cui, J. Chen. Adv. Energy Mater. 2014, **4**, 1400337(1-8). (b) A. Kong, Q. Lin, C. Mao, X. Bu, P. Feng, Chem. Commun., 2014, **50**, 15619-15622.

9) a) O. M. Yaghi, M. O'Keeffe, N. W. Ockwig, H. K. Chae, M. Eddaoudi and J. Kim, Nature, 2003, **423**, 705-714 (b) N. W. Ockwig, O. D. Friederichs, M. O'Keeffee and O. M. Yaghi, Acc. Chem. Res., 2005, **38**, 176-182 (c) S. Kitagawa, R. Kitaura and S. I. Noro, Angew. Chem. Int. Ed., 2004, **43**, 2334-2375 (d) C. N. R. Rao, S. Natarajan and R. Vaidhyanathan, Angew. Chem. Int. Ed., 2004, **43**, 1466-1496.

10) B. H. Ye, M. L. Tong, X. M. Chen, Coord. Chem. Rev., 2005, **249**, 545-565.

11) Y. B. Go, X. Wang, E. V. Anokhina, A. J. Jacobson, Inorg. Chem., 2005**, 44**, 8265-8271.

12) Bruker, SMART, Bruker AXS Inc., Madison, Wisconsin, USA, **2002**.

13) Bruker, SAINT and SADABS, Bruker AXS Inc., Madison, Wisconsin, USA, **2008**.

14) SHELXL, G. M. Sheldrick, ActaCryst.,2008, **112**, A64.

15) D. Briggs, M. P. Sech, Practical Surface Analysis; Wiley: New York, USA, **1983**, 119.

16) X. Li, X. Sun, X. Li and X. Xu, New J. Chem., 2015 (DOI: 10.1039/C5NJ00706B)

17) (a) Y. B. Go, X. Wang, E. V. Anokhina and A. J. Jacobson, Inorg. Chem., 2004, **43**, 5360-5367. (b) Y. J. Song, P. Zhang, J. W. Ji and Z. B. Han, Russian J. Cord, Chem., 2009, **35**, 698-703. (c). L. N. Zhu, L. Z. Zhang, W. Z. Wang, D. Z. Liao, P. Cheng, Z. H. Jiang and S. P. Yan, Inorg. Chem. Commun., 2002, **5**, 1017–1021.

18) H. Ma, J. L. Petersen, V. G. Young Jr., G. T. Yee and M. P. Jensen, J. Am. Chem. Soc., 2011, **133**, 5644–5647.

19) D. Cheng, M. A. Khan and R. P. Houser, J. Chem. Soc., Dalton Trans., 2002, 4555–4560.

20) E. A. Owen and D. M. Jones, Proceedings of the Physical Society, London, 1954, **67**, 456-466.

21) Z. J. Huba and E. E. Carpenter, Dalton Trans., 2014, **43**, 12236–12242.

22) G. Will, N. Masciocchi, W. Parrish and M. Hart, J. App. Cryst., 1987, **20**, 394-401.

23) W. C. Ren, F. Li, J. Chen, S. Bai and H.M. Cheng, Chem. Phys. Lett., 2002, **359**, 196–202.

24) F. Tuinstra, J. L. Koenig, J. Chem. Phys., 1970, **53**, 1126–1130.

25) M. C. Biesinger, B. P. Payne, A. P. Grosvenor, L. W. M. Lau, A. R. Gerson, R. St. C. Smart, Appl. Surf. Sci., 2011, **257**, 2717-2730.

26) N. L. Torad , M. Hu, S. Ishihara, H. Sukegawa, A. A. Belik, M. Imura, K. Ariga, Y. Sakka and Y. Yamauchi, Small, 2014, **10**, 2096–2107.

27) C. Yi, S. Jiang ;C. Nanxian, Solid State Commun., 2009, 149, 121-125.

28) S. S. Rao and T. R. Ananthraman, Current Sci., 1963, **32**, 262-263.

29) J. Zeng, Q. Zhang, J. Chen, Y. Xia, Nano Lett., 2010, **10**, 30-35.

30) Z. D. Pozun, S. E. Rodenbusch, E. Keller, K. Tran, W. Tang, K. J. Stevenson, G. Henkelman. J. Phys. Chem. C, 2013, **117**, 7598−7604.

31) Y. Lu, Y. Mei, M. Drechsler and M. Ballauff, Angew. Chem. Int. Ed., 2006, **45**, 813-816.

32) B. Todic, V. V. ordomsky, N. M. Nikacevic, A. Y. Khodakov and D. B. Bukur, Catal. Sci. Technol., 2015, **5**, 1400-1411.

VITA

Siddharth Gopalakrishnan was born in Kumbakonam, Tamil Nadu on June 12th, 1992. In May 2009, he graduated from Maharishi Vidya Mandir Senior secondary school. In fall 2009, he joined the undergraduate program in Chemical Engineering at St. Joseph's College of Engineering under Anna University, Chennai, Tamil Nadu. He graduated with a Bachelor of Technology degree in Chemical Engineering in spring 2013.

In fall 2013, he enrolled for a master's degree in Chemical Engineering at Missouri University of Science and Technology. At Missouri S&T, he carried out research work under the guidance of Dr. Amitava Choudhury and Dr. Xinhua Liang, on surface active transition metal catalyst. He also served as Treasurer for India Association at Missouri S&T. He graduated with a Master of Science in Chemical Engineering from Missouri University of Science and Technology in December 2015.